RADIATION RESEARCH **181**, 284–292 (2014)
0033-7587/14 $15.00

DOI: 10.1667/RR13303.1

Generalized Time-Dependent Model of Radiation-Induced Chromosomal Aberrations in Normal and Repair-Deficient Human Cells

Artem L. Ponomarev,[a,b,1] Kerry George[c] and Francis A. Cucinotta[b,2]

[a] *Division of Space Life Sciences, Universities Space Research Association, Houston, Texas 77058;* [b] *NASA Lyndon B. Johnson Space Center, Space Radiation Program, Houston Texas 77058; and* [c] *Wyle Science, Technology & Engineering Group, Houston, Texas 77058*

Ponomarev, A. L., George, K. and Cucinotta, F. A. Generalized Time-Dependent Model of Radiation-Induced Chromosomal Aberrations in Normal and Repair-Deficient Human Cells. *Radiat. Res*. 181, 284–292 (2014).

We have developed a model that can simulate the yield of radiation-induced chromosomal aberrations (CAs) and unrejoined chromosome breaks in normal and repair-deficient cells. The model predicts the kinetics of chromosomal aberration formation after exposure in the G_0/G_1 phase of the cell cycle to either low- or high-LET radiation. A previously formulated model based on a stochastic Monte Carlo approach was updated to consider the time dependence of DNA double-strand break (DSB) repair (proper or improper), and different cell types were assigned different kinetics of DSB repair. The distribution of the DSB free ends was derived from a mechanistic model that takes into account the structure of chromatin and DSB clustering from high-LET radiation. The kinetics of chromosomal aberration formation were derived from experimental data on DSB repair kinetics in normal and repair-deficient cell lines. We assessed different types of chromosomal aberrations with the focus on simple and complex exchanges, and predicted the DSB rejoining kinetics and misrepair probabilities for different cell types. The results identify major cell-dependent factors, such as a greater yield of chromosome misrepair in ataxia telangiectasia (AT) cells and slower rejoining in Nijmegen (NBS) cells relative to the wild-type. The model's predictions suggest that two mechanisms could exist for the inefficiency of DSB repair in AT and NBS cells, one that depends on the overall speed of joining (either proper or improper) of DNA broken ends, and another that depends on geometric factors, such as the Euclidian distance between DNA broken ends, which influences the relative frequency of misrepair.

INTRODUCTION

Many experimental studies have been conducted on radiation-induced chromosomal aberrations (CAs), including mechanistic studies, biodosimetry, genomic instability and investigations of possible biomarkers for carcinogenesis (*1–9*) [for historical review of this field of research see ref. (*56*)]. Chromosomal aberrations are prevalent in tumors and are likely related to cancer risk, and data on CA yields have been used as a cancer biomarker (*10*). One of the difficulties of assessing chromosome damage experimentally is the lack of an available technique that can provide a high-resolution assessment of all types of chromosomal rearrangements simultaneously. Computerized simulations can provide predictions of CAs in their entirety and can predict the presence of damage that is below the resolution of current cytogenetic techniques (*2, 8*). Therefore, models may provide valuable information for mechanistic studies and assessment of radiation risk.

The first version of the current model (*11, 12*) was introduced as a part of the NASA Radiation Track Image package (NASARTI, http://spaceradiation.usra.edu/irModels/) to assess acute irradiation of the human genome after low- or high-LET radiation exposures (*11, 12, 39–43*). This model was then updated to provide predictions of all types of CAs (translocations, deletions, inversions, complex aberrations, dicentrics and rings) induced at first cell division after acute irradiation in the G_0/G_1 phase of the cell cycle (*56*). The model is limited to chromosome-type exchanges and is currently unable to simulate chromatid-type aberrations (*57*), which are more prevalent in repair-deficient cell lines.

In this article, we show the latest revision of the model, which introduces a time dependence to simulate the kinetics of CAs formation after radiation exposure. This time dependence was introduced through a time constant that varies with cell type, reflecting individual repair efficiency. The time constant determines the overall speed of repair, whereas the reaction rates (*48*) for properly repaired DSBs and misrepaired DSBs (*13, 14*) determine the quality of repairs and, ultimately the kinetics of CA formation. In this time-dependent model, not all chromosome breaks will rejoin by the simulated time T (which can be chosen to

[1] Address for correspondence: NASA Lyndon B. Johnson Space Center, ATTN: Mail code SK, 2101 NASA Parkway, Houston, TX 77058; e-mail: artem.l.ponomarev@nasa.gov.

[2] Current address: University of Nevada Las Vegas, Department of Health Physics and Diagnostic Sciences, Las Vegas, NV 89154.

TABLE 1
Parameters for the Empirical Bimodal Curves [Eq. (2)] used as Experimental Data in Model Fits

Parameter	HF/highLET	HF/lowLET	AT/highLET	AT/lowLET
A	0.8	0.5	0.8	0.5
B	0.2	0.5	0.2	0.5
τ_1	0.5	0.5	2.0	2.0
τ_2	2.0	2.0	8.0	8.0

Notes. HF cells are wild-type; AT cells are repair deficient. High-LET radiation was iron ions, $E = 1{,}000$ MeV/u, $D = 1$ Gy. Low-LET radiation was gamma radiation, $D = 1$ Gy.

equal the experimental time), and this new property widens the scope of CAs to include DNA fragments and terminal deletions. The algorithm proceeds in a series of steps, each corresponding to a time interval, which can then be defined by fitting the model to the experimental data. As the algorithm progresses, the number of DSBs decreases, as fragments either rejoin correctly (that is, the topology of a chromosome is restored by restituting the DNA free ends from one DSB; hereinafter referred to as ''rejoin'') or rejoin to form aberrant chromosomes (hereinafter referred to as ''misrejoin''), or remain unrejoined. The choice of terminology was dictated by the model resolution limit of 2 kb. It has been proposed that small fragments of DNA may be missing at the site of DNA repair (possibly a few bp in length), but as this is below the resolution limit of the current model, such restituted breaks are considered rejoined. Results from the model were then compared to experimental data, sometimes fitted as bimodal exponential decay curves, to determine the adjustable time constant. At any simulated time a cell can have any of the following: intact chromosomes, linear aberrant chromosomes, rings and unrejoined fragments. Therefore, the spectrum of CAs and unrejoined fragments can be evaluated for a given time after exposure and this evaluation provides a more accurate comparison with the experimental data.

Experimental data using fibroblast cells deficient in ATM (product of gene mutations in ataxia telangiectasia patients) or NBS (product of *gene mutations* in Nijmegen breakage syndrome) show that DSB repair deficiencies affect the yield of radiation-induced CAs and the rate of DSB rejoining is faster in normal cells than in repair-deficient cells. In addition, we show here the modeled kinetics of high- and low-LET radiation-induced chromosome exchanges in repair-deficient and normal human fibroblast cells.

MATERIALS AND METHODS

Model of the Human Genome

The NASARTI model, used to reconstruct interphase chromosomes in a Monte Carlo approach, produces a simulated set of radiation-induced DNA fragments similar to those induced by particle tracks. This model has been described in detail in previous publications (*11, 12, 33, 48*). Here we recap the previous model description that pertains only to the current, time dependent model (*33, 42, 43*).

Stochastic Model of Chromosomal Aberrations

The model algorithm generates simulated CAs using a Monte Carlo simulation of DSB rejoining/misrejoining as described previously (*13, 48*). The initial state in the system is an array of DSB locations (x, y, z, λ), where x, y and z are the physical coordinates of DSBs and λ is genomic distance (measured in DNA base pairs). The algorithm uses parameters P and I as the DSB free end joining reaction rates of repair and misrepair. I depends on the Euclidian distance and P was set to unity, as the ratio of intact chromosomes to aberrant chromosomes depends on the ratio I/P (the ratio of the misrejoining rate to the rejoining rate), in which I is a Gaussian function of the Euclidian distance between the reacting DSB free ends [Eq. (1)]. That is, P can be absorbed in Z in Eq. (1). A pair of DSB free ends is selected and either joined or rejected [Eq. (1)] until the next iteration, where they can be reselected and possibly paired in a different way and 1 may participate in other joinings. The function for I is expressed as

$$I = \frac{1}{Z} e^{-\frac{r^2}{\sigma^2}}, \tag{1}$$

where Z is an empirically calibrated parameter, r is a Euclidian distance between reacting DSB free end (μm) and σ is an adjustable parameter with the dimension of microns.

The optimal values for the reaction rates were calibrated using experimental data. This process allows proper repair to dominate, which is consistent with experimental data. From our previous kinetic models *(13, 26)* we expect a different, competing first-order process to occur leading to residual unrejoined breaks, but this is expected to have a minor influence on the prediction of exchanges. We plan to study this process in future work.

Classification of Chromosomal Aberrations

The bookkeeping and the classification of the CAs and the treatment of centromeres are described in a previous article (*48*). Unrepaired fragments and terminal deletions, which can be generated in the new time-dependent model, were not considered in the earlier version of the model that focused exclusively in CA. The new version of the model produces relative frequencies of CAs, as well as probability density functions for the size distribution of a given type of aberration, simulated at the experimental time (or at some previous time, as will be shown later). Complex aberrations, which are defined as a group of exchanges that involve at least 3 DSBs and at least 2 chromosomes and can be modeled with the help of a sub-algorithm as described previously (*48*).

DSB Rejoining/Misrejoining Kinetics

The model was updated to consider the time dependence of DNA DSB rejoining/misrejoining, in which individual cell types have different yields of residual DSBs that do not undergo rejoining or misrejoining. DSB repair kinetics are usually best fit as bimodal

TABLE 2
Model Results for τ, σ and *Z*

	HF/lowLET	HF/highLET	AT/lowLET	AT/highLET	NBS/lowLET	NBS/highLET
τ,h	1.20×10–3	1.44×10–3	7.50×10–3	1.88×10–3	1.00×10–3	8.25×10–4
σ^2, μm	2.00×103	2.00×103	2.00×103	2.00×103	2.00×103	2.00×103
Z	50	50	5	50	50	50

Notes. The physical time (τ) associated with one iteration in the program and σ and *Z* are the parameters in Eq. (1). HF cells are wild-type; AT and NBS cells are repair deficient. High-LET radiation was iron ions, $E = 1{,}000$ MeV/u, $D = 1$ Gy. Low-LET radiation was gamma radiation, $D = 1$ Gy.

exponential curves with two time constants that depend on the cell type and the quality of radiation [Eq. (2)],

$$N(t) = N_0[Ae^{-\frac{t}{\tau_1}} + Be^{-\frac{t}{\tau_2}}] \quad (2)$$

where $N_0 \approx 25$ DSBs/Gy in G_0/G_1. Table 1 shows the parameters used for noncycling human fibroblasts exposed to low-LET and high-LET radiations and for repair-deficient AT cells. For NBS cells, we did not use the bimodal curves, instead, we used data in a tabular format from Girard *et al*. (*44*).

Simulation of Kinetics of Aberration Formation

The relative yields of exchanges change with time after an acute radiation exposure, as the process of chromosome repair progresses and progressively more breaks become rejoined (*20, 21, 30, 36–38*). In the model the evolution of this system proceeds in incremental steps, as pairs of DSB free ends are chosen randomly and either rejoin, misrejoin or are rejected according to the rejection rate 1-*I*, which we call an elementary step in the program. A time constant was assigned to these steps by fitting the model to data on the kinetics of DSB rejoining (*28*), allowing us to track the evolution of CAs and intact chromosomes.

RESULTS

Model Fits to Experimental Data on DSB Kinetics and Model Set-up

For the time-dependent updates to the model, we calibrated the physical time τ, corresponding to one elementary step in the program, using data on DSB repair kinetics (*47*). Results are shown in Table 2. The other two parameters, *Z* and σ (*48*) were refitted also. The optimal parameters of the model, *Z*, σ and τ are different for different cell types and different radiation types (Table 2). A typical σ value corresponds to a radius for DSB interaction of roughly 0.9 μm (for comparison, the diameter of the nucleus in this example is 12 μm). This is also very close to the result reported by Rydberg *et al*. (*50*), who determined the interaction radius to be 0.5 μm. The normalization constant *Z* [Eq. (1)] regulates the overall frequency of misrejoinings to accommodate the lower number of aberrations relative to the number of intact chromosomes reported in the experimental data (*47*). A steep drop-off in the Gaussian function indicates that, for binary misrejoinings, the radius of interaction is small, about the size of a chromosomal domain (*22*). We believe the preponderance of proper rejoinings after an acute irradiation is due to the close proximity of the free ends produced by one DSB (*49*). This simulated rate of rejoinings is independent of any repair process and is simply a way of allowing proper rejoinings to dominate which is in line with experimental data.

We accommodated the effect of slower kinetics of DSB repair in repair-deficient cells than in normal cells by assigning an adjustable time unit per iteration of the CA formation algorithm. The same effect can be achieved by readjusting *P* and *I* simultaneously, *P* can be assigned a value of less than one and *I* can be adjusted proportionately to keep *I*/*P* constant. However, to be consistent with the previous versions of the model, we elected to keep the same values for *P* and *I* and introduced τ as the physical time interval corresponding to an iteration. The values of τ, obtained from model fits, were relatively small (Table 2), since the program produces a large number of iterations to reach the state corresponding to experimental data derived 24 h after exposure. This large number of iterations is due to small *I* and therefore, a high rejection rate of elementary moves (an elementary move is the selection of a DSB free end pair and assignment of one of the 3 possible outcomes, as explained above).

The model fits to experimental DSB restitution kinetic curves are shown in Fig. 1. The experimental curves are described by bimodal exponents with two time constants, τ_1 and τ_2 [Eq. (2) and Table 1], corresponding to the slow-restituting groups and the fast-restituting groups of DSBs respectively (*14, 17, 24, 51–55*). The constants *A* and *B* determine the relative contribution of each type of DSB restitution process (Table 1). We do not insist that such bimodal curves are the best technique to fit the experimental data, we simply use them as a way to extrapolate empirical data to multiple data points generated by our mechanistic model with a stochastic process for CA formation. The excellent agreement of the model with DSB restitution kinetics data determines the physical duration of a single step of the Monte Carlo code.

The model has different sensitivity to the parameters τ, σ and *Z*. The physical time unit (τ) associated with one elementary step in the program, has the most influence on the model output. This time parameter is fitted to DSB rejoining kinetics, as discussed above and determines how fast a cell can repair DNA damage. The other two adjustable parameters, σ and *Z* (to which the model is less sensitive) somewhat influence the characteristics of the CA spectrum,

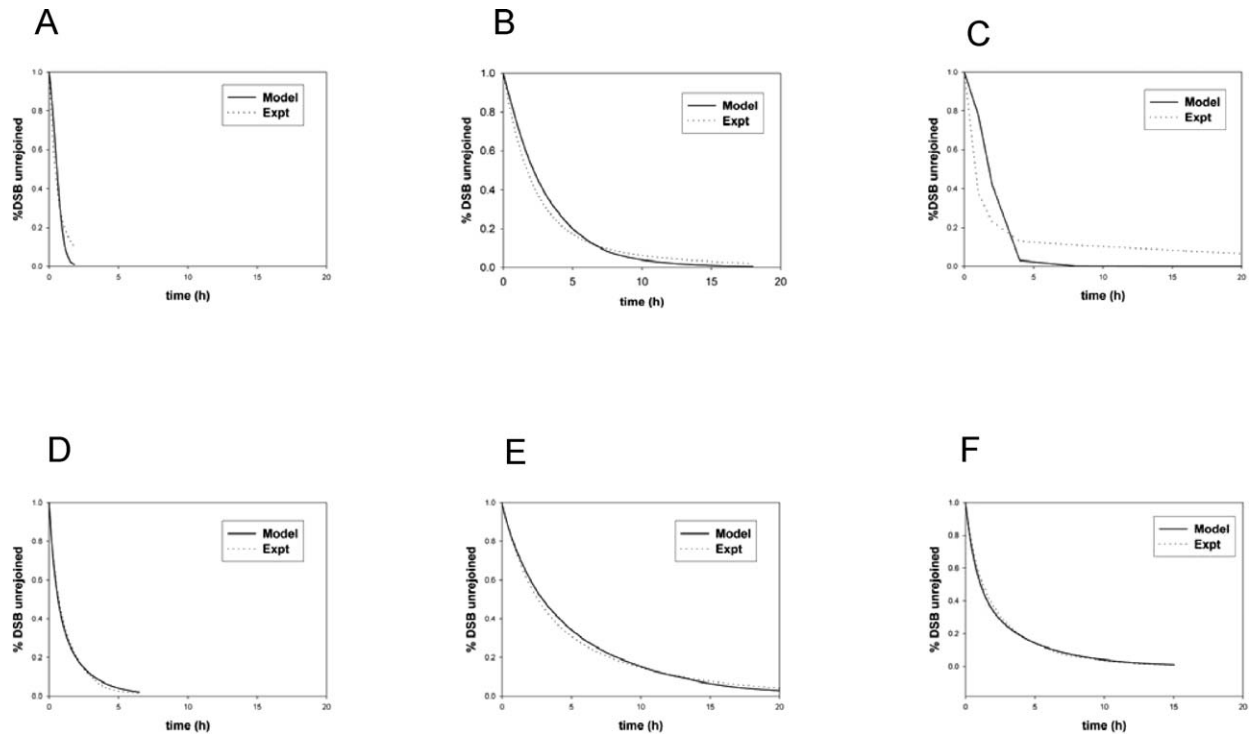

FIG. 1. Percentage of unrejoined DSBs, according to the model and comparison to the bimodal exponential curve (bi-exp) based on experimental data, for different cell types and high- and low-LET radiations. (Panels describe what case was compared: cell type, radiation type and dose.) Panel A: HF cells (wild-type), gamma radiation, $D = 1$ Gy; panel B: AT cells (repair deficient), gamma radiation, $D = 1$ Gy; panel C: NBS cells (repair deficient), gamma radiation, $D = 1$ Gy. The experimental data were obtained in a tabular format (*44, 46*). Panel D: HF cells (wild-type), Fe ions, $E = 1{,}000$ MeV/u, $D = 1$ Gy; panel E: AT cells (repair deficient), Fe ions, $E = 1{,}000$ MeV/u, $D = 1$ Gy; panel F: NBS cells (repair deficient), Fe ions, $E = 1{,}000$ MeV/u, $D = 1$ Gy. The experimental data were obtained in a tabular format (*44, 46*).

rather than the overall frequency of CAs or how fast they form.

Once the time parameter was determined, we refined the overall stochastic process of rejoining/misrejoining to focus on the frequency of misrepair. Misrepair is controlled by the I function, which has two adjustable parameters, σ and Z. The ''radius of interaction'' σ, described above, has the least influence on the model output. The Z parameter is responsible for the overall frequency of misrepair and has a somewhat larger influence (higher sensitivity) on the output. A comparison of these parameters in Table 2 leads us conclude that AT cells are overall slower than normal human fibroblast (HF) cells to repair DNA damage. NBS cells are also slower than HF cells, but not as slow as AT cells. The misrepair frequency I (calculated from σ and Z) is somewhat higher for AT cells than NBS cells. Additional analysis is presented in the Discussion section.

Data from experimental studies of NBS cells are usually presented in a tabular form, rather than the bi-exponential format (*44, 46, 47*). In Fig. 1C and F, we compare the model fits to the experimental data for NBS cells. Experiments have shown that the mean rejoining rate in NBS cells is only slightly slower than the rate in wild-type cells, whereas AT cells have much slower rejoining rates than the wild-type (*44, 46*).

Model Fits to Experimental Data on Chromosome Aberrations

All types of chromosome exchanges can be quantified with the model, but for comparison with the experimental data from George *et al*. (*47*), we focused on simple reciprocal exchanges between two chromosomes and complex aberrations involving the interaction of three or more breaks on two or more chromosomes. The simulated dose response for simple and complex exchanges induced by γ rays in normal human fibroblast cells and the corresponding experimental data (*47*) are shown in Figs. 2A and B and 3A and B. Experimental analysis was conducted 24 h after exposure and model predictions for this time point mostly agree with the results with the exception of the relatively rare complex aberrations in wild-type cells.

Data in Figs. 2 and 3 show dose-response values for CAs in AT cells (panels B and E) after exposure to radiation from γ rays and high-LET iron ions, respectively. AT cells have higher yields of radiation-induced exchanges per unit dose than normal cells.

Figure 2C and F and Fig. 3C and F show dose-response values for simplex complex CAs in NBS cells. The experimental data were taken from Girard *et al*. (*44*), Pluth *et al*. (*46*) and George *et al*. (*47*). The biological

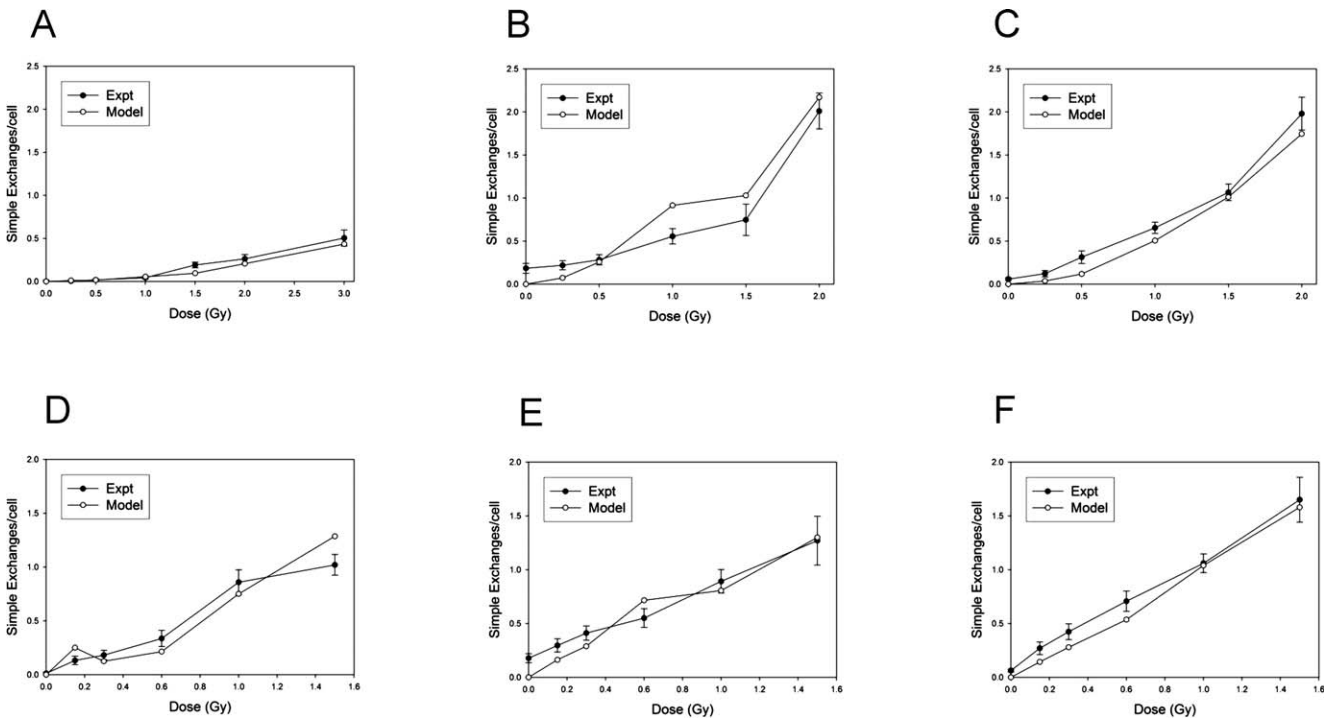

FIG. 2. Dose dependence of the number of simple exchanges is compared for the experimental data and the model, for different cell types and high- and low-LET radiations. The experimental data are shown as closed circles and the model data are shown as open circles. The exposure time, $T = 24$ h. Panel A: Number of simple exchanges in HF cells exposed to gamma radiation. Panel B: Number of simple exchanges in AT cells exposed to gamma radiation. Panel C: Number of simple exchanges in NBS cells exposed to gamma radiation. Panel D: Number of simple exchanges in HF cells exposed to Fe ions, $E = 1{,}000$ MeV/u. Panel E: Number of simple exchanges in AT cells exposed to Fe ions, $E = 1{,}000$ MeV/u. Panel F: Number of simple exchanges in NBS cells exposed to Fe ions, $E = 1{,}000$ MeV/u.

mechanisms of repair deficiency in the NBS cells are quite different from those in AT cells, as the experiment indicates. Table 2 shows this phenomenon numerically, the simulation constants were quite different for the two repair-deficient cell types. When the simulated yields of exchanges are matched to the experimental analysis time, the data were close to the reported experimental data for both low- and high-LET radiations (Figs. 2C, F and 3C, F).

Simulation of the CA Dynamics by the Time-Dependent Model

Figure 4 shows the modeled yields of translocations at different times after exposure and predicts that translocations develop rapidly in normal human cells after low- or high-LET radiation. For repair-efficient cells (HF), the majority of exchanges develop at $T = 2$ h. Repair-deficient cells (AT and NBS) show gradual dynamics in CA development. The model predicts that slightly fewer γ-ray-induced translocations occur at earlier times after exposure for repair-deficient cells (Fig. 4A, B and C), indicating that these translocations take more time to develop in comparison to the wild-type. This trend is consistent with the data for high-LET Fe ions (Fig. 4D, E and F).

DISCUSSION

The robustness of our model allows the entire damaged genomic system to be assessed as it evolves in time after acute radiation through a process of repair and misrepair of DNA, leading to either intact chromosomes, transitory breaks (meaning those that can participate in joining further) or final CAs. It should be noted, however, that this strength is offset by the fact that at this stage of modeling we did not consider chromatid-type aberrations. Both chromosome and chromatid-type aberrations are produced at first mitosis in repair-deficient cells after irradiation in the G_0/G_1 phase of the cell cycle, whereas only chromosome aberrations are produced in wild-type cells. The chromatid-type aberrations might be important for the understanding of the repair defects in mutant cells. Such an insight into the mechanism of DNA repair deficiency will require an upgrade of the current version of the program to model chromatid exchanges and will be explored in future studies. Until that time we believe the comparison of chromosome yields in both cell types is still important and is the best approach, given the current limitations of the model. Similar but slightly different modeling approaches have been published in the literature (*24–27, 32, 58–60*). However, our current model is unique because it includes chromatin structure, which is important for the study of high-LET radiation, and

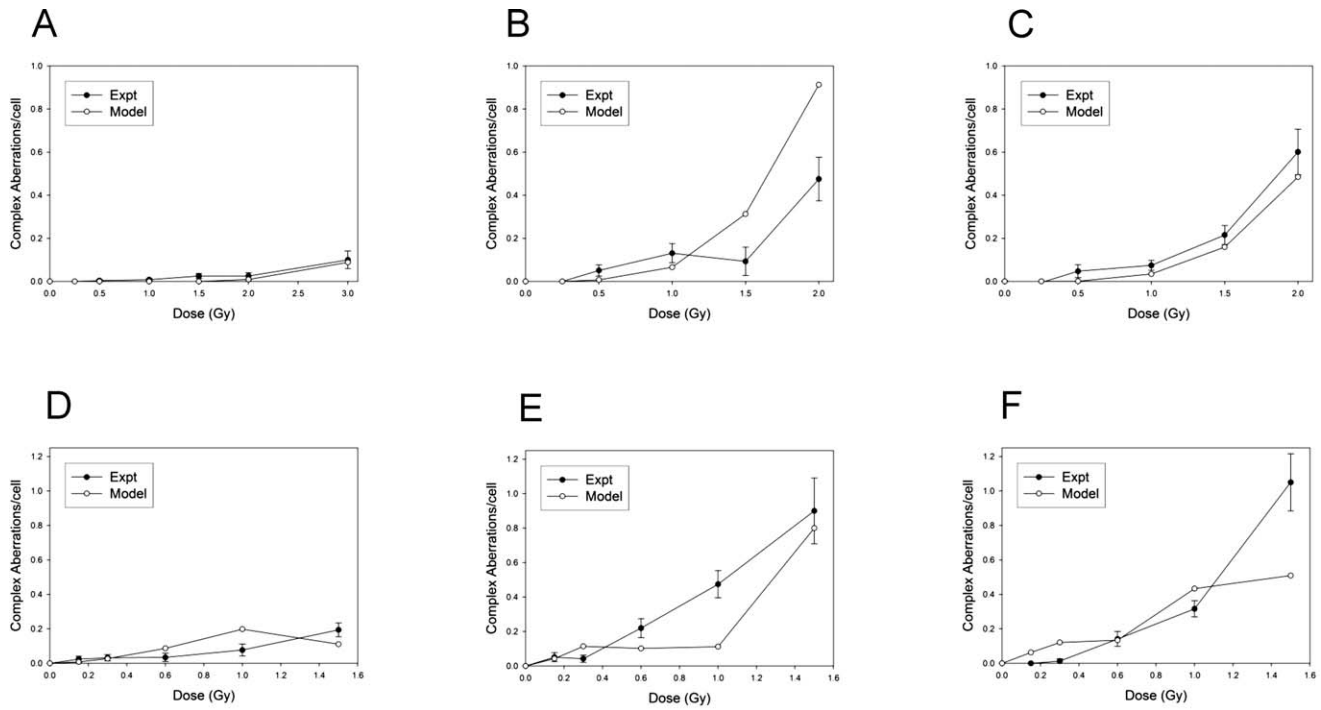

FIG. 3. Dose dependence of the number of complex aberrations per cell is compared for the experimental data and the model, for different cell types and high- and low-LET radiations. The experimental data are shown as closed circles and the model data are shown as open circles. The exposure time, $T = 24$ h. Panel A: Number of complex aberrations per cell in HF cells exposed to gamma radiation. Panel B: Number of complex aberrations per cell in AT cells exposed to gamma radiation. Panel C: Number of complex aberrations per cell in NBS cells exposed to gamma radiation. Panel D: Number of complex aberrations per cell in HF cells exposed to Fe ions, $E = 1{,}000$ MeV/u. Panel E: Number of complex aberrations per cell in AT cells exposed to Fe ions, $E = 1{,}000$ MeV/u. Panel F: Number of complex aberrations per cell in NBS cells exposed to Fe ions, $E = 1{,}000$ MeV/u.

our model has a more transparent mechanism for the formation of CAs. The Monte Carlo algorithm provides the frequency and size distribution of any type of CA.

Our model has three adjustable parameters, which might give the impression that it can be easily fitted to experimental data, but has a weak predicting power for the number of CAs. However, there is an implicit constraint on the parameter σ, as this describes the geometric range of interaction between remote DSBs, which obviously has to be less than the nucleus diameter and close to a domain size. Simulations show that the sensitivity of the model on Z is also small. The low sensitivity of the model on σ and Z can also be predicted since I has to be small regardless of the cell type, as the number of misrejoinings is always less the number of correct rejoinings. The parameter that can change the result dramatically is the time constant τ, the value of which is not determined from CA distributions, but from DSB restitution kinetics. Thus, τ is determined by experimental data other than CA studies and is then no longer an adjustable parameter for CA data fitting.

The novelty of this version of the model is the time-dependent algorithm that allows us to analyze the evolution of CAs over time in repair-efficient cells (wild-type) and repair-deficient cells with different repair mechanisms. The CAs can accumulate early in the experiment, as they do in HF cells, or they might continue developing gradually with time and result in a relatively higher yield of CAs, as in AT and NBS cells.

Results from our previous work suggest that an alternative model could be considered, in which a competing first-order reaction occurs with the rate constant k_{fix} and an initial parameter estimate of 0.1 (*13*). This slower competing reaction leads directly to DNA fragments, including terminal deletions of different sizes. These two competing reactions result in preferential fragment sizes because of the geometric factors that arise in the first reaction described above, whereas the competing first-order reaction contains no geometric information. This alternative model will be considered in future work and should be important for model predictions of terminal deletions.

It has been hypothesized that the NBS and AT repair defects are linked to either a higher probability of misrejoining or a one-hit mechanism and not to a slower DSB rejoining rate. The impact of repair deficiency on the rejoining rate can be seen in the τ values shown in Table 2 and in experimental data (*44*). Our data seem to support the hypothesis that the NBS defect is linked to a one-hit mechanism. The rates of PCC break or DNA damage foci disappearance are similar for AT and wild-type cells (*16, 61*), indicating that DSB rejoining rates are similar for these cells. Our data does not generally support except for the high-LET case, that the ratio of τ's for AT cells to HF cells

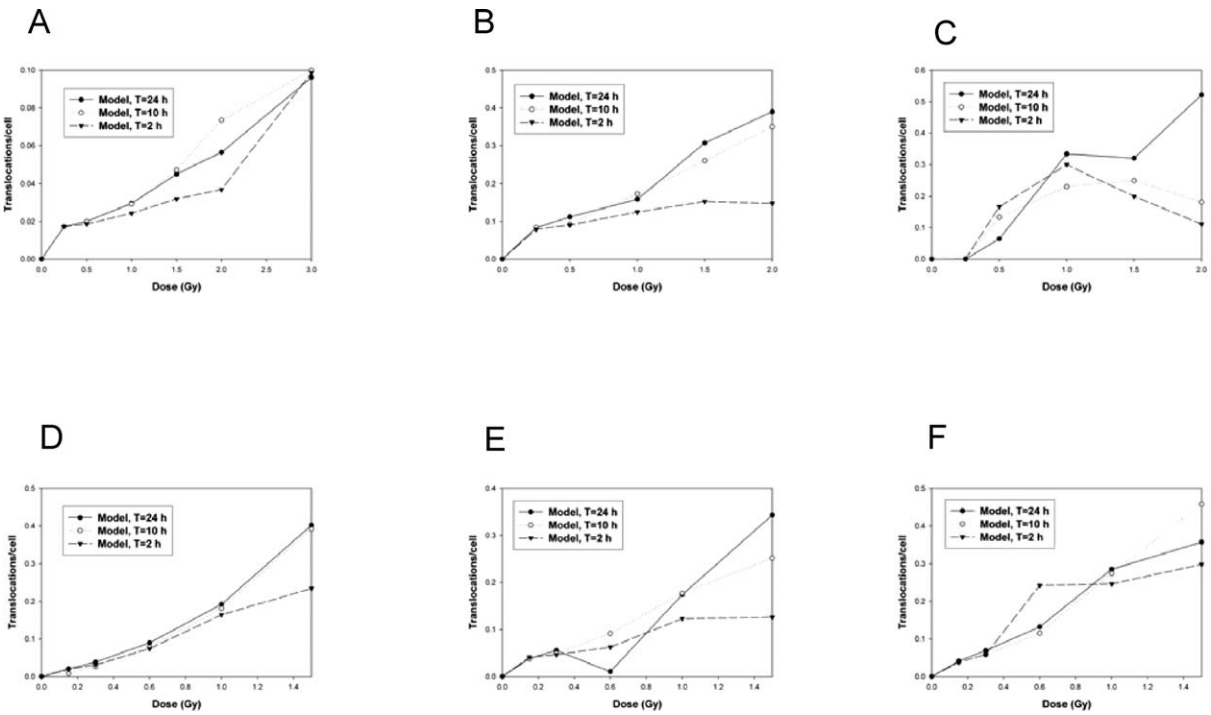

FIG. 4. Dose dependence of the number of translocations per cell, according to the model, for different cell types and high- and low-LET radiations, and the modeled sensitivity to simulated experimental time (2, 10 and 24 h) at $D = 1$ Gy. The actual experiment was conducted at 24 h after exposure. Panel A: Number of translocations per cell expected in HF cells exposed to gamma radiation. Panel B: Number of translocations per cell expected in AT cells exposed to gamma radiation. Panel C: Number of translocations per cell expected in NBS cells exposed to gamma radiation. Panel D: Number of translocations per cell expected in HF cells exposed to Fe ions, $E = 1{,}000$ MeV/u. Panel E: Number of translocations per cell expected in AT cells exposed to Fe ions, $E = 1{,}000$ MeV/u. Panel F: Number of translocations per cell expected in NBS cells exposed to Fe ions, $E = 1{,}000$ MeV/u.

is only 1.31, indicating that slowing of the repair kinetics for AT cells is not too pronounced under high-LET conditions. However, some AT experimental data do show dissimilarity different DSB rejoining rates after high- and low-LET irradiation (*62*).

Our model suggests that several mechanisms could exist for the inefficiency of DSB repair in AT and NBS cells, with one mechanism depending on the overall speed of joining (proper or improper) of DNA broken ends and the fidelity of rejoining, and another mechanism depending on the geometric factors, such as the Euclidian distance between DNA broken ends, which has also been shown to influences the relative frequency of misrepair.

CONCLUSIONS

We have designed a mechanistic model that fits experimental data of both the DSB rejoining kinetics and the yields of CAs in wild-type and DSB repair-deficient cells. The model can also be used to predict the yield of exchanges at timepoints that is matched to the timing of the experimental observations. Moreover, the model can extrapolate the yield of exchanges to time periods before the experimental observations were conducted, thus revealing how CA yields evolve in time. The model results associate major cell-dependent factors with higher CA misrepair in AT cells and slower rejoinings in NBS cells, relative to the wild-type.

ACKNOWLEDGMENTS

Funding was provided through the NASA Space Radiation Risk Assessment Project. Special thanks to Dr. Michael Cornforth for useful discussions.

Received: January 5, 2013; accepted: December 19, 2013; published online: March 10, 2014

REFERENCES

1. Cucinotta FA, Durante M. Cancer risk from exposure to galactic cosmic rays: implications for space exploration by human beings. Lancet Oncol 2006; 7:431–5.
2. Cornforth MN, Bailey SM, Goodwin EH. Dose responses for chromosome aberrations produced in noncycling primary human fibroblasts by alpha particles, and by gamma rays delivered at sublimiting low dose rates. Radiat Res 2002; 158:43–53.
3. Geard CR. Charged particle cytogenetics: effects of LET, fluence, and particle separation on chromosomal aberrations. Radiat Res 1995; 104:S112–21.
4. Geard CR, Colvett RD, Rohrig N. On the mechanics of chromosomal aberrations. A study with single and multiple spatially-associated protons. Mutat Res 1980; 69:81–99.
5. Hada M, Huff JL, Patel Z, Kawata T, Pluth JM, George KA, Cucinotta FA. AT cells are not radiosensitive for chromosomal exchanges at low dose. Mutat Res 2011; 716:76–83.

6. Gahdhi M, Dillon LW, Pramanik S, Nikiforov YE, Wang Y-H. DNA breaks at fragile sites generate oncogenic RET/PTC rearrangements in human thyroid cells. Oncogene 2010; 29:2272–80.
7. Cucinotta FA, Kim M-HY, Willingham V, George KA. Physical and biological organ dosimetry analysis for International Space Station astronauts. Radiat Res 2008; 170:127–38.
8. George K, Durante M, Willingham V, Wu H, Yang T, Cucinotta FA. Biological effectiveness of accelerated particles for the induction of chromosome damage measured in metaphase and interphase human lymphocytes. Radiat Res 2003; 160:425–35.
9. George K, Cucinotta FA. The influence of shielding on the biological effectiveness of accelerated particles for the induction of chromosome damage. Adv Space Res 2007; 39:1076–81.
10. Bonassi S, Norppa H, Ceppi M, Strömberg U, Vermeulen R, Znaor A, et al. Chromosomal aberration frequency in lymphocytes predicts the risk of cancer: results from a pooled cohort study of 22 358 subjects in 11 countries. Carcinogenesis 2008; 29:1178–83.
11. Ponomarev AL, Huff J, Cucinotta FA. The analysis of the densely populated patterns of radiation-induced foci by a stochastic, Monte Carlo model of DNA double strand breaks induction by heavy ions. Int J Radiat Biol 2010; 86:507–15.
12. Ponomarev AL, Costes SV, Cucinotta FA. Stochastic properties of radiation induced DSBs: DSB distributions in large scale chromatin loops, the HPRT gene and within the visible volumes of DNA repair foci. Int J Radiat Biol 2008; 84:916–29.
13. Cucinotta FA, Nikjoo H, O'Neill P, Goodhead DT. Kinetics of DSB rejoining and formation of simple chromosomes exchange aberrations. Int J Radiat Biol 2000; 76:1463–74.
14. Sachs RK, Hahnfeld P, Brenner DJ. Review. The link between low-LET dose-response relations and the underlying kinetics of damage production/repair/misrepair. Int J Radiat Biol 1997; 72:351–74.
15. Ma Y, Pannicke U, Schwarz K, Lieber MR. Hairpin opening and overhang processing by an Artemis/DNA-dependent protein kinase complex in nonhomologous end joining and V(D)J recombination. Cell 2002; 108:781–94.
16. Riballo E, Kühne M, Rief N, Doherty A, Smith GCM, Recio M-J, et al. A pathway of double-strand break rejoining dependent upon ATM, Artemis, and proteins locating to γ-H2AX foci. Mol Cell 2004; 16:715–24.
17. Radivoyevitch T. Time course solutions of the Sax-Markov binary eurejoining/misrejoining model of DNA double-strand breaks. Radiat Environ Biophys 2000; 39:265–73.
18. Münkel C, Eils R, Dietzel S, Zink D, Mehring C, Wedemann G, et al. Compartmentalization of interphase chromosomes observed in simulation and experiment. J Mol Biol 1999; 285:1053–65.
19. Radivoyevitch T, Hoel DG, Chen AM, Sachs RK. Misrejoining of double-strand breaks after X irradiation: relating moderate to very high doses by a Markov model. Radiat Res 1998; 149:59–67.
20. Zou Y, Gryaznov SM, Shay JW, Wright WE, Cornforth MN. Asynchronous replication timing of telomeres at opposite arms of mammalian chromosomes. Proc Natl Acad Sci U S A 2004; 101:12928–33.
21. Bailey SM, Cornforth MN. Telomeres and DNA double-strand breaks: ever the twain shall meet? Cell Mol Life Sci 2007; 64:2956–64.
22. Ballarini F, Merzagora M, Monforti F, Durante M, Gialanella G, Grossi GF, et al. Chromosome aberrations induced by light ions: Monte Carlo simulation based on mechanistic model. Int J Radiat Biol 1999; 75:7535–46.
23. Martinez-Lopez W, Folle GA, Cassina G, Mendez-Acuna L, Di-Tomaso MV, Obe G, et al. Distribution of breakpoints induced by etoposide and X-rays along the CHO X chromosome. Cytogenet Genome Res 2004; 104:182–7.
24. Moiseenko VV, Edwards AA, Nikjoo N. Modelling the kinetics of chromosome exchange formation in human cells exposed to ionising radiation. Radiat Environ Biophys 1996; 35:31–5.
25. Holley WR, Mian IS, Park SJ, Rydberg B, Chatterjee A. A model for interphase chromosomes and evaluation of radiation-induced aberrations. Radiat Res 2002; 158:568–80.
26. Cucinotta FA, Pluth JM, Anderson JA, Harper JV, O'Neill P. Biochemical kinetics model of DSB repair and induction of gamma-H2AX foci by non-homologous end joining. Radiat Res 2008; 169:214–22.
27. Lucas JN, Poggensee M, Straume T. Translocations between two specific human chromosomes detected by three-color ''chromosome painting.'' Cytogen Cell Genet 1993; 62:11–2.
28. Durante M, Furusawa Y, Majima H, Kawata T, Gotoh E. Association between G2-phase block and repair of radiation-induced chromosome fragments in human lymphocytes. Radiat Res 1999; 151:670–6.
29. Wolff S. The repair of X-ray-induced chromosome aberrations in stimulated and unstimulated human lymphocytes. Mutat Res 1972; 15:435–44.
30. Natarajan AT, Balajee AS, Boei JJ, Darroudi F, Dominguez I, Hande MP, et al. Mechanisms of induction of chromosomal aberrations and their detection by fluorescence in situ hybridization. Mutat Res 1996; 372:247–58.
31. Savage JR. On the nature of visible chromosomal gaps and breaks. Cytogenet Genome Res 2004; 104:46–55.
32. Friedland W, Paretzke HG, Ballarini F, Ottolenghi A, Kreth G, Cremer C. First steps towards systems radiation biology studies concerned with DNA and chromosome structure within living cells. Radiat Environ Biophys 2008; 47:49–61.
33. Ponomarev AL, Cucinotta FA, Sachs RK, Brenner DJ, Peterson LE. Extrapolation of the DNA fragment-size distribution in a high-dose PFGE assay to low doses. Radiat Res 2001; 156(5 Pt 2): 594–7.
34. Lieberman-Aiden E, van Berkum NL, Willams L, Imakaev M, Ragoczy T, Telling A, et al. Comprehensive mapping of long-range interactions reveals folding principles of the human genome. Science 2009; 326:289–93.
35. Anderson RM, Stevens DL, Goodhead DT. M-FISH analysis shows that complex chromosome aberrations induced by α-particle tracks are cumulative products of localized rearrangements. Proc Natl Acad Sci U S A 2002; 99:12167–72.
36. Boei JJ, Vermeulen S, Natarajan AT. Technical report. Analysis of radiation-induced chromosomal aberrations using telomeric and centromeric PNA probes. Int J Radiat Biol 2000; 76:163–7.
37. Mestres M, Caballin MR, Schmid E, Stephan G, Sachs R, Barrios L, Barquinero JF. Analysis of α-particle induced chromosome aberrations in human lymphocytes, using pan-centromeric and pan-telomeric probes. Int J Radiat Biol 2004; 80:737–44.
38. Durante M, George K, Cucinotta FA. Chromosomes lacking telomeres are present in the progeny of human lymphocytes exposed to heavy ions. Radiat Res 2006; 165:51–8.
39. Rydberg B. Radiation-induced heat-labile sites that convert into DNA double-strand breaks. Radiat Res 2000; 153:805–12.
40. Stenerlöw B, Höglund E, Carlsson, J. DNA fragmentation by charged particle tracks. Adv Space Res 2002; 30:859–63.
41. Stenerlöw B, Karlsson KH, Cooper B, Rydberg B. Measurement of prompt DNA double-strand breaks in mammalian cells without including heat-labile sites: results for cells deficient in nonhomologous end joining. Radiat Res 2003; 159:502–10.
42. Radulescu I, Elmroth K, Stenerlöw B. Chromatin organization contributes to non-randomly distributed double-strand breaks after exposure to high-LET radiation. Radiat Res 2004; 161:1–8.
43. Höglund E, Blomquist E, Carlsson J, Stenerlöw B. DNA damage induced by radiation of different linear energy transfer: initial fragmentation. Int J Radiat Biol 2000; 76:539–47.
44. Girard P-M, Foray N, Stumm M, Waugh A, Riballo E, Maser RS,

et al. Radiosensitivity in Nijmegen breakage syndrome cells is attributable to a repair defect and not cell cycle checkpoint defects. Cancer Res 2000; 60:4881–8.

45. Costes SV, Ponomarev AL, Chen JL, Nguyen D, Cucinotta FA, Barcellos-Hoff MH. Image-based modeling reveals dynamic redistribution of DNA damage into nuclear sub-domains. PLoS Comput Biol 2007; 3:e155.

46. Pluth JM, Yamazaki V, Cooper BA, Rydberg BE, Kirchgessner CU, Cooper PK. DNA double-strand break and chromosomal rejoining defects with misrejoining in Nijmegen breakage syndrome cells. DNA Repair (Amst) 2008; 7:108–18.

47. George KA, Hada M, Jackson LJ, Elliott T, Kawata T, Pluth JM, Cucinotta F. Dose response of γ rays and iron nuclei for induction of chromosomal aberrations in normal and repair-deficient cell lines. Radiat Res 2009; 171:752–63.

48. Ponomarev AL, George K, Cucinotta FA. Computational model of chromosome aberration yield induced by high- and low-LET radiation exposures. Radiat Res 2012; 177:727–37.

49. Du G, Drexler GA, Friedland W, Greubel C, Hable V, Krücken R, et al. Spatial dynamics of DNA damage response protein foci along the ion trajectory of high-LET particles. Radiat Res 2011; 176:706–15.

50. Rydberg B, Cooper B, Cooper PK, Holley W, Chatterjee A. Dose-dependent misrejoining of radiation-induced DNA double-strand breaks in human fibroblasts: experimental and theoretical study for high- and low-LET radiation. Radiat Res 2005; 163:526–34.

51. Kawata T, Gotoh E, Durante M, Wu H, George K, Furusawa Y, Cucinotta FA. High-LET radiation-induced aberrations in prematurely condensed G2 chromosomes of human fibroblasts. Int J Radiat Biol 2000; 76:929–37.

52. Durante M, Furusawa Y, George K, Gialanella G, Greco O, Grossi G, et al. Rejoining and misrejoining of radiation-induced chromatin breaks. IV. Charged particles. Radiat Res 1998; 149:446–54.

53. Stenerlöw B, Hoglund E, Carlsson J, Blomquist E. Rejoining of DNA fragments produced by radiations of different linear energy transfer. Int J Radiat Biol 2000; 76:549–57.

54. Greinert R, Volkmer B, Virsik-Peuckert RP, Harder D. Comparative study of the repair kinetics of chromosomal aberrations and DNA strand breaks in proliferating and quiescent CHO cells. Int J Radiat Biol 1996; 70:33–43.

55. Foray N, Badie C, Alsbeih G, Fertil B, Malaise EP. A new model describing the curves for repair of both DNA double-strand breaks and chromosome damage. Radiat Res 1996; 146:53–60.

56. Bedford JS, Dewey WB. Historical and current highlights in radiation biology: Has anything important been learned by irradiating cells? Radiat Res 2002; 158:251–91.

57. Little JB, Nagasawa H, Dahlberg WK, Zdzienicka MZ, Burma S, Chen DJ. Differing responses of Nijmegen breakage syndrome and ataxia telangiectasia cells to ionizing radiation. Radiat Res 2002; 158:319–26.

58. Alloni D, Campa A, Friedland W, Mariotti L, Ottolenghi A. Track structure, radiation quality and initial radiobiological events: Considerations based on the PARTRAC code experience. Int J Radiat Biol 2012; 88:77–86.

59. Friedland W, Kundrat P, Jacob P. Stochastic modeling of DSB repair after photon and ion irradiation. Int J Radiat Biol 2012; 88:129–36.

60. Friedland W, Jacob P, Kundrat P. Mechanistic simulation of radiation damage to DNA and its repair: on the track towards systems radiation biology modelling. Radiat Prot Dosimetry 2011; 143: 542–8.

61. Strasser H, Grabenbauer GG, Sprung CN, Sauer R, Distel LVR. DNA double-strand break induction and repair in irradiated lymphoblastoid, fibroblast cell lines and white blood cells from ATM, NBS and radiosensitive patients. Strahlenther Onkol 2007; 8: 447–53.

62. Kitajima S, Nakamura H, Adachi M, Ijichi K, Yasui Y, Saito N, et al. AT cells show dissimilar hypersensitivity to heavy-ion and X-rays irradiation. J Radiat Res 2010; 51: 251–5.